Energy 67 (2014) 548–556

Contents lists available at ScienceDirect

Energy

journal homepage: www.elsevier.com/locate/energy

Thermodynamic analysis of an in-cylinder waste heat recovery system for internal combustion engines

Sipeng Zhu [a], Kangyao Deng [a,*], Shuan Qu [b]

[a] Key Laboratory for Power Machinery and Engineering of Ministry of Education, Shanghai Jiao Tong University, Shanghai City 200240, China
[b] China North Engine Research Institute, Datong 037036, China

ARTICLE INFO

Article history:
Received 17 September 2013
Received in revised form
27 January 2014
Accepted 1 February 2014
Available online 22 February 2014

Keywords:
Internal combustion engine
Waste heat recovery
Steam injection
Intake valve close timing
Thermal efficiency

ABSTRACT

In this paper, an in-cylinder waste heat recovery system especially for turbocharged engines is proposed to improve the thermal efficiencies of internal combustion engines. Simplified recovery processes can be described as follows: superheated steam generated by engine waste heat is injected into the pipe before the turbine to increase the boost pressure of the fresh air; intake valve close timing is adjusted to control the amount of fresh air as the original level, and thus the higher pressure charged air expands in the intake stroke and transfers the pressure energy directly to the crankshaft. In this way, the increased turbine output by the pre-turbine steam injection is finally recovered in the cylinder, which is different from the traditional Rankine cycle. The whole energy transfer processes are studied with thermodynamic analyses and numerical simulations. The results show that the mass flow rate of the injected steam has the biggest influence on the energy transfer processes followed by the temperature of the injected steam. With this in-cylinder waste heat recovery system, the fuel economy of a selected turbocharged diesel engine can be improved by 3.2% at the rated operating point when the injected mass flow ratio is set to be 0.1.

1. Introduction

With the problems of energy and environment becoming more and more serious, depending solely on improving the combustion process in the cylinder cannot fulfill people's higher requirement for the thermal efficiency of the ICE (internal combustion engine). Since more than half of the fuel energy is taken away by the exhaust gas and cooling water, WHR (waste heat recovery) technologies show great potentialities of improving the fuel economy and reducing the CO_2 emissions.

There are mainly three kinds of WHR techniques including the thermoelectrical generator, compounding turbo and Rankine cycle, which have their own advantages and disadvantages. Hussain et al. [1] and Yu et al. [2] conducted simulation and experimental researches on exhaust heat recovery with thermoelectric generators, which demonstrated the potential of this technique for automotive industry. Hountalas et al. [3] examined effects of the mechanical and electrical compounding turbo on the fuel economy, power output, and pollutant emissions. Arias et al. [4] and Boretti [5] showed interests in applying the Rankine cycle on hybrid cars due to the flexible energy management system. Ringler et al. [6] confirmed the Rankine cycle can provide an additional power output of about 10% on a gasoline engine. Briggs et al. [7] demonstrated a thermal efficiency of 45% on a light duty diesel engine with the organic Rankine cycle. Yu et al. [8] indicated that the organic Rankine cycle can improve the thermal efficiency of a diesel engine by 6.1% with the exhaust gas and jacket water as waste heat sources. Gao et al. [9] proposed that the Rankine cycle system with a reciprocating piston expander can increase the engine power output by 12% when a high speed turbocharged diesel engine operates at 80 kW/2590 r/min. In general, the thermoelectrical generator has the advantages of free maintenance, silent operation, high reliability and involving no moving and complex mechanical parts, while its high cost of thermoelectrical materials and the low recovery efficiency (normally lower than 4%) restrict the application on ICEs [10]. The compounding turbo transfers the surplus pressure energy of the exhaust gas into mechanical power, which adds the pumping loss and has limited operating conditions [11]. For the Rankine cycle, a potential fuel economy improvement around 10% has been demonstrated by many manufacturers [12], but its high cost, big size and complicated configuration still need to be improved.

* Corresponding author. Tel./fax: +86 021 34206380.
E-mail addresses: kydeng@sjtu.edu.cn, sipengzhu@126.com (K. Deng).

http://dx.doi.org/10.1016/j.energy.2014.02.006
0360-5442/

Nomenclature

cp	specific heat capacity [kJ/kg K]
D	Mass flow ratio [–]
h	specific enthalpy [kJ/kg]
$\dot{I}$	exergy destruction rate [kW]
$\dot{m}$	mass flow rate [kg/s]
P	pressure [bar]
$\dot{Q}$	heat flow [kW]
s	specific entropy [kJ/kg K]
T	temperature [K]
ΔT	temperature difference [K]
$\dot{W}$	power [kW]
x	mole ratio [–]

Greek symbols

π	pressure ratio [–]
η	efficiency [%]

Subscripts

c	compressor
exh	exhaust gas
eva	evaporation
max	maximum
p	pump
t	turbine
w	water
0–5, 0′–6′	state points in waste heat recovery system

Abbreviation

BMEP	brake mean effective pressure
BSFC	brake specific fuel consumption
CA	crank angle
IVC	intake valve close
NOx	nitride oxides

Different from those typical WHR techniques, many new recovery strategies have been reported in recent years [13–20]. Conklin and Szybist [13] presented a concept of adding two additional strokes to the Otto or Diesel engine cycle to increase the fuel efficiency. The research results showed that the two-stroke steam cycle can add an additional power stroke by recovering waste heat from the engine coolant and exhaust gas with water injection and expansion. Fu et al. [14] designed an open steam power cycle for exhaust gas energy recovery on a four-cylinder naturally aspirated engine with the last cylinder used for steam expansion, which made the Otto or Diesel cycle couple with the open Rankine cycle on ICEs. The outcomes indicated that the maximum bottoming cycle power can reach 19.2 kW and the thermal efficiency can be improved by 6.3% at 6000 r/min. Serrano et al. [15] performed a theoretical investigation on coupling the Rankine cycle WHR system with a two-stage turbocharged diesel engine. New alternative solutions that the Rankine cycle supplied the recovered energy directly to the low pressure compressor were studied, and the results showed that those alternative layouts produce lower benefits in fuel consumption compared to that obtained in the conventional Rankine cycle. Fu et al. [16] continued to propose a steam turbocharging system to boost the engine intake pressure instead of the traditional exhaust turbocharging system. The results indicated that the engine power can be improved by as much as 7.2%, and thermal efficiencies can be improved by 2 percent points or more in the high speed range. Liu et al. [17]compared various means of bottoming cycles for exhaust gas energy recovery including direct secondary expansion, over-heated and standard Rankine steam cycles and Brayton cycles with or without regeneration. Shu et al. [18] analyzed the combined thermoelectric generator and organic Rankine cycle used in exhaust heat recovery of the ICE theoretically. Yamada and Mohamad [19] proposed an open Rankine cycle subsystem on a hydrogen ICE which produces nearly three times more water than a conventional engine. He et al. [20] demonstrated more waste heat can be recovered with combined thermodynamic cycles, which consist of an organic Rankine cycle for recovering waste heat of lubricant and exhaust gas and a Kalina cycle for recovering waste heat of cooling water.

To transfer the Rankine cycle expander output into useful power, there are two typical alternatives including directly linking the expander shaft with the crankshaft and converting the mechanical power into electrical power [11]. Both of those two alternatives are not easy to be achieved, which has become a main obstacle for the Rankine cycle utilization. Thus Serrano et al. [15] and Fu et al. [16] tried to connected the Rankine cycle turbine shaft directly to the compressor shaft and replaced the traditional turbocharging system to boost the charge air as mentioned above.

In this paper, a novel concept is proposed to reintroduce the waste heat of the exhaust gas into the cylinder with the pre-turbine steam injection and the adjustment of IVC (intake valve close) timing. The main purpose of this study is to verify the feasibility and the potential benefits of this new in-cylinder WHR system. The structure and principles of the new system are presented first, and then the whole recovery system is divided into two subsystems for theoretical analyses. Thermodynamic models based on the first and second laws of thermodynamics are built in Matlab software to analyze the energy and exergy transfer processes and effects of injected parameters on the recovery efficiency. The main operating parameters of a selected diesel engine equipped with this new WHR system are evaluated under full load operating conditions with a calibrated model in GT-power software.

2. System description and thermodynamic analysis

2.1. System description

Fig. 1 shows the layout of the in-cylinder WHR system for a turbocharged engine. The main working processes can be described as follows. As the working fluid, water is compressed to a certain

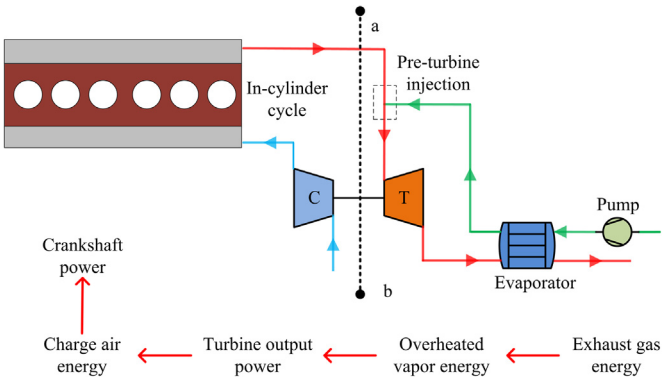

Fig. 1. Layout and principle of the in-cylinder waste heat recovery system.

pressure in the pump and then flows into the evaporator, where it is heated into superheated steam by the exhaust gas. The exhaust gas out of the exhaust manifold and the injected superheated steam mix in the pipe before the turbine and form a gas-steam mixture ("wet gases" for short). Wet gases then flow into the turbine, and the turbine output power increases obviously due to the increased mass flow rate. The expanded wet gases flow through the evaporator accompanied with the heat exchange process and finally discharge into the environment. The increased turbine output power boosts the charge air pressure, which converts the mechanical power into pressure energy of the charge air. By advancing or delaying the IVC timing, the amount of fresh air can be controlled at the same level of the original operating condition to guarantee a steady operation of the ICE. Finally, the waste heat energy recovered from the exhaust gas transfers to the crankshaft by the expansion process of the high pressure charge air during the intake stroke in the cylinder. The whole waste heat transfer processes can be explained with the flow diagram in Fig. 1.

In order to analyze the energy transfer processes, the in-cylinder WHR system is divided into two subsystems by the dotted line "ab" as shown in Fig. 1. The right side is called exhaust gas WHR subsystem, and the left side is named in-cylinder cycle subsystem. Those two subsystems are connected with each other by the exhaust manifold and the turbocharger shaft.

2.2. Exhaust gas WHR subsystem

Fig. 2 shows the schematic diagram and the T–s diagram of the exhaust gas WHR subsystem. For the thermodynamic models of this subsystem, the inlet of the exhaust gas can be regarded as a boundary condition with a constant mass flow rate, and the outlet is the environment condition. For simplicity, the pressure drops in the evaporator and pipes can be neglected compared with that of the turbine, and there is no heat transfer between every component and the environment. Combined with the T–s diagram, the subsystem can be described as follows.

Pumping process: The actual and isentropic pumping processes of the water are described as 0′–1′ and 0′–1's in the T–s diagram, respectively. The power consumed by the pump is given as

$$\dot{W}_p = \dot{m}_w(h_{1's} - h_{0'})/\eta_p \tag{1}$$

where $\dot{m}_w$ is the mass flow rate of water, and η_p is the isentropic efficiency of the pump.

Heat absorption process: Liquid water is superheated into steam from state point 1′ to 2′ when it flows through the evaporator. Since the temperature of point 2′ is lower than that of point 4 due to the temperature difference between hot and cold sides of the evaporator, evaporation efficiency η_{eva} is introduced to indicate the relationship between $T_{2'}$ and T_4 and can be calculated by

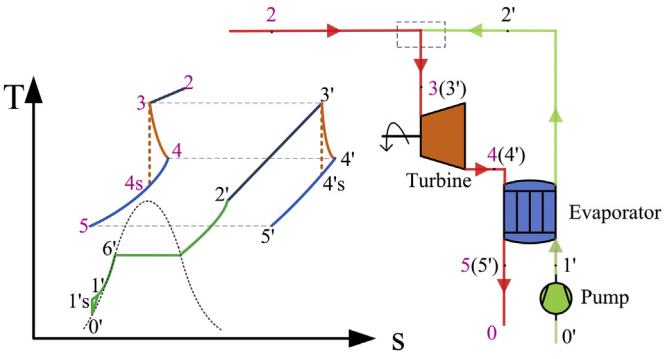

Fig. 2. Sketch and T–s diagram of the exhaust gas waste heat recovery subsystem.

$$\eta_{eva} = (T_{2'} - T_{1'})/(T_4 - T_{1'}) \tag{2}$$

Mixing process: The superheated steam is injected into the pipe before the turbine and mixes with the exhaust gas out of the exhaust manifold, corresponding to the processes of 2′–3′ and 2–3. Due to the temperature difference between state points 2 and 2′, superheated steam keeps on absorbing heat from the exhaust gas, and finally those two fluids reach a same temperature before flowing into the turbine. Injected mass flow ratio D and molar flow ratio x are defined to simplify the analyses and expressed as

$$D = \dot{m}_w/\dot{m}_{exh} \tag{3}$$

$$x = D(M/M') \tag{4}$$

where $\dot{m}_{exh}$ is the mass flow rate of the exhaust gas, M and M' are the molar mass of the exhaust gas and water. According to the energy conservation, the mixing process can be described as

$$h_2 - h_3 = D(h_{3'} - h_{2'}) \tag{5}$$

Expansion process: After the mixing process, the wet gases flow into the turbine and then expand, corresponding to the processes of 3′–4′ and 3–4. Since the partial pressure is relatively low and the temperature is very high, steam before the turbine can be treated as the ideal gas. With the ideal gas law, the expansion ratio of the turbine after the steam injection can be calculated by

$$\pi_{t'} = (1+x)\pi_t T_3/T_2 \tag{6}$$

where π_t and $\pi_{t'}$ are the expansion ratios of the turbine before and after the steam injection. Since the gas composition is changed with the steam injection, the isentropic exponent and the isobaric heat capacity can be expressed as

$$\kappa_{mix} \approx \frac{1}{1+x}\kappa_{exh} + \frac{x}{1+x}\kappa_w \tag{7}$$

$$c_{p,mix} = \frac{1}{1+D}c_{p,exh} + \frac{D}{1+D}c_{p,w} \tag{8}$$

where κ_{exh}, κ_w, $c_{p,exh}$ and $c_{p,w}$ are the average isentropic exponent and the average isobaric heat capacity of the exhaust gas and the superheated steam in the corresponding temperature range. It is worth mentioned that Eq. (7) is a simplified formula [21]. Assuming the isentropic efficiency η_t of the turbine is constant, the output power $\dot{W}_t$ and the outlet temperature T_4 of the turbine can be calculated by

$$\dot{W}_t = (1+D)\dot{m}_{exh}c_{p,mix}(T_3 - T_4) \tag{9}$$

$$T_4 = T_3\left(1 - \eta_t\left(1 - \pi_{t'}^{\frac{1-\kappa_{mix}}{\kappa_{mix}}}\right)\right) \tag{10}$$

Processes 3–4s and 3′–4′s are the isentropic expansion processes of the exhaust gas and the superheated steam. With the same expansion ratio and the different isentropic exponents, the final temperature of the exhaust gas after the isentropic expansion is lower than that of the superheated steam. To guarantee the same temperature of the exhaust gas and the superheated steam, the actual expansion process must be accompanied with the heat absorption process of the exhaust gas and the heat release process of the superheated steam.

Heat release process: The wet gases after expanding flow through the evaporator and heat the liquid water into superheated

steam corresponding to the processes of 4–5 and 4′–5′. The heat transfer process in the evaporator can be described as

$$(1+D)c_{p,\mathrm{mix}}(T_4-T_5) = D(h_{2'}-h_{1'}) \tag{11}$$

In this study, the exhaust gas utilization efficiency η_{exh} is adopted for the subsystem performance evaluation and can be computed as

$$\eta_{\mathrm{exh}} = \frac{\dot{W}}{\dot{Q}} = \frac{\dot{W}_t - \dot{W}_p}{\dot{m}_{\mathrm{exh}}c_{p,\mathrm{exh}}(T_2-T_0)} \tag{12}$$

It is impossible to convert all the waste heat of the exhaust gas into useful power due to the irreversibility of the heat transfer and power processes in subsystem components. In order to study influences of primary parameters on the subsystem irreversibility destruction, exergy analyses based on the second law of thermodynamics are necessary to be conducted.

Assuming the subsystem reaches a steady state, the exergy destruction rate of every process can be expressed as

$$\dot{I} = T_0\frac{\mathrm{d}s_g}{\mathrm{d}t} = \dot{m}T_0\left[\sum_{\mathrm{out}} s - \sum_{\mathrm{in}} s - \sum_k \frac{q_k}{T_k}\right] \tag{13}$$

where T_0 is the environmental temperature, T_k is the temperature of each heat source, q_k is the heat transferred from each heat source to the control volume. The exergy destruction rates of heat transfer and power processes are composed of the following parts: the exergy destruction rate $\dot{I}_p$ of the pumping process, the exergy destruction rate $\dot{I}_{\mathrm{mix}}$ of the mixing process, the exergy destruction rate $\dot{I}_t$ of the expansion process, the exergy destruction rate $\dot{I}_{\mathrm{eva}}$ of the evaporating process and the exergy destruction rate $\dot{I}_{\mathrm{exh}}$ of the discharging process. Without considering the heat transfer between every system component and the environment, those different kinds of exergy destruction rates can be calculated with Eq. (14)–(18).

$$\dot{I}_p = \dot{m}_w T_0(s_{1'}-s_{0'}) \tag{14}$$

$$\dot{I}_{\mathrm{mix}} = \dot{m}_{\mathrm{exh}}T_0[(s_3-s_2)+D(s_{3'}-s_{2'})] \tag{15}$$

$$\dot{I}_t = \dot{m}_{\mathrm{exh}}T_0[(s_4-s_3)+D(s_{4'}-s_{3'})] \tag{16}$$

$$\dot{I}_{\mathrm{eva}} = \dot{m}_{\mathrm{exh}}T_0[(s_5-s_4)+D(s_{5'}-s_{4'})+D(s_{2'}-s_{1'})] \tag{17}$$

$$\dot{I}_{\mathrm{exh}} = \dot{m}_{\mathrm{exh}}T_0\left[(s_0-s_5)+D(s_{0'}-s_{5'})+\frac{h_5-h_0+D(h_{5'}-h_{0'})}{T_0}\right] \tag{18}$$

2.3. In-cylinder cycle subsystem

To figure out the principle of this in-cylinder WHR system, working processes in the cylinder are necessary to be investigated. Fig. 3 shows the ideal P–V diagrams of the conventional diesel engine cycle and the new in-cylinder cycle adopted in this WHR system. By advancing the IVC timing, the amount of fresh air is controlled at the same level as the original operating condition. With an expansion of the charge air after the intake valve is closed before the BDC (bottom dead centre), the temperature and pressure at the BDC are lower than those of the conventional cycle, which also means low-temperature processes in the following strokes. A same effect can be obtained with delaying the IVC timing. Without the adjustment of the IVC timing, the increased charge pressure will bring too much fresh air into the cylinder, which leads to a much higher peak firing pressure.

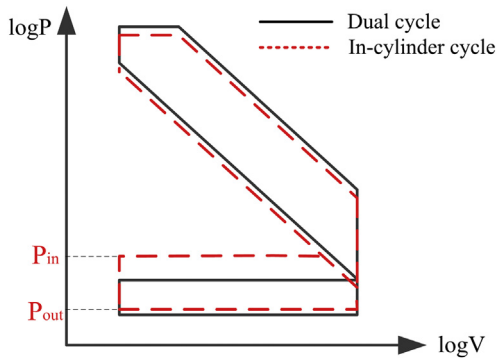

Fig. 3. P–V diagrams of the diesel engine cycle and the new in-cylinder cycle.

As can be seen, the in-cylinder cycle of this WHR system is similar to the Miller cycle, which is originally proposed by Miller to increase the output power of ICEs [22]. The Miller cycle can also achieve higher thermal efficiencies and lower NOx (nitride oxides) emissions due to the low temperature in the cylinder, and a lot of related researches have been reported in recent years [23–27]. Tinschmann et al. [23] adopted a medium degree Miller timing (IVC = 25°CA (crank angle) before BDC) combined with an increased compression ratio and an improved single-stage turbocharging system to fulfill the IMO Tier 2 NOx limits with no change in fuel consumption. Tagai et al. [24] also confirmed the potentials of the Miller cycle on the NOx emissions and fuel economy for the marine diesel engines. Kim et al. [25] compared effects of the Miller cycle with advancing and delaying IVC strategies, and the results showed that extreme late Miller cycle seriously deteriorate engine performances at low load and starting conditions. Niemi et al. [26] indicated that the retarded IVC strategy cannot work well within the entire load-speed operating conditions. Okamoto et al. [27] indicated that the Miller cycle together with other measures can increase the BMEP (brake mean effective pressure) and the thermal efficiency of a lean burn gas engine dramatically.

Compared with the early IVC strategy, the late IVC strategy brings the benefits of in-cylinder charge air motion. But the early IVC strategy is still used in the following simulation considering the low load conditions as mentioned in Refs. [25,26]. Advancing the IVC timing is always achieved with reduced maximum valve lift owing to mechanical limitations for the valve acceleration and the valve-piston clearance at the TDC (top dead centre), while delaying the IVC timing is always realized by increasing the dwell of the maximum valve lift [26].

Different from the Miller cycle, the high boost pressure in this WHR system is achieved with the pre-turbine steam injection not by increasing the back pressure before the turbine. As shown in Fig. 3, the exhaust back pressure may slightly increase due to the increase of the mass flow rate and the decrease of the temperature before the turbine according to Eq. (6). Thus a large positive pumping power is obtained in this WHR system. In this way, the waste heat of the exhaust gas is transferred to the superheated steam, then to the charge air and finally be recovered in the cylinder.

3. Methods

3.1. Constraint of the evaporator

An important design parameter of the evaporator is the MTD (minimum temperature difference) of the fluids between the hot

and cold sides. A small MTD decreases the irreversibility of the heat transfer process and increases the cost and structural complexity of the evaporator, while a big MTD deteriorates the heat transfer flux in the evaporator. Fig. 4 shows the temperature curves of the cold and hot fluids in the evaporator. It can be seen that the MTD can only occur at the inlet and outlet of the evaporator and the pinch point at which the evaporating process starts. When the mass flow rate of water is too large, the MTD occurs at the inlet point of the liquid water, and the superheated state cannot be guaranteed due to the large evaporation enthalpy of water. When the mass flow rate is too small, the MTD occurs at the outlet point of the superheated steam, and the temperature drop of the exhaust gas in the hot side is too small, which decreases the exhaust gas utilization efficiency. For a reasonable choice of the mass flow rate, the MTD normally occurs at the pinch point of the evaporating process, just as shown in Fig. 4.

At the same time, the outlet temperature of wet gases should be kept larger than 90 °C to protect the evaporator from fouling [28]. To decrease the thermal stress of the high temperature region of the evaporator, the outlet temperature of the superheated steam should not be too high. Meanwhile the temperature difference between the hot and cold fluids in the evaporator should be small to reduce the exergy destruction. So the MTD should also occur at the pinch point of the evaporating process from the perspectives of the evaporator design and exergy destruction.

According to the energy balance of evaporating and superheating processes, the relationship between the steam mass flow rate and the superheating temperature can be described as

$$(1+D)c_{p,\mathrm{mix}}(T_4 - T_{6'} - \Delta T_{\min}) = D(h_{2'} - h_{6'}) \tag{19}$$

where $\Delta T_{\min}$ is the MTD of the evaporator. Under the constraint of the MTD, the relationship between D and η_{eva} can be easily acquired with Eqs. (3) and (19).

Meanwhile the MTD should always keeps larger than 10 K to insure the driving force of the heat transfer process in the evaporator. Also when the engine is operated in extremely low load conditions, the exhaust gas temperature may not be sufficient to superheat water into steam, thus pre-turbine stream injection cannot be adopted.

3.2. Calculated algorithm of the exhaust gas WHR subsystem

For the exhaust gas WHR subsystem, the most important parameters are the mass flow rate, the temperature and the pressure of the injected steam, which determine the exhaust gas utilization efficiency. To study the influences of those injected parameters on the recovery efficiency and exergy destruction, thermodynamic models were established in Matlab with the analyses in Section 2.

The initial values were listed as follows: the initial temperature and pressure of the exhaust gas were set to be 850 K and 2.3 bar, which were test under the rated operating condition of a six-cylinder turbocharged diesel engine; the environment temperature and pressure were fixed at 300 K and 1.01 bar; the isentropic efficiencies of the turbine and the pump were assumed to be 0.7 and 0.8, respectively. The properties of water were calculated with REFPROP [29], which was developed by the National Institute of Standards and Technology of the United States.

It is worth mentioned that the exhaust gas mass flow rate was not given because the injected mass flow ratio can indicate it if the steam mass flow rate was fixed. Also the pressure and temperature before the turbine always change simultaneously with the variation of the engine load. Since evaluations of injected parameters under different exhaust gas conditions would lead similar results, only one inlet boundary of the exhaust gas was evaluated in the following analyses. Before the analyses of the exhaust gas WHR subsystem, the temperature and pressure of every state point should be calculated with those initial values, and the calculated algorithm is shown in Fig. 5.

3.3. Simulation model of the in-cylinder cycle subsystem

In order to obtain accurate results which were closer to the actual operating conditions, the in-cylinder model was established

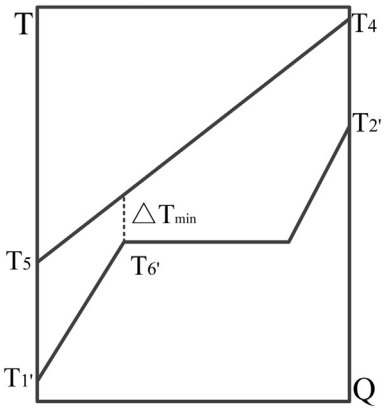

Fig. 4. Temperature curves in the evaporator.

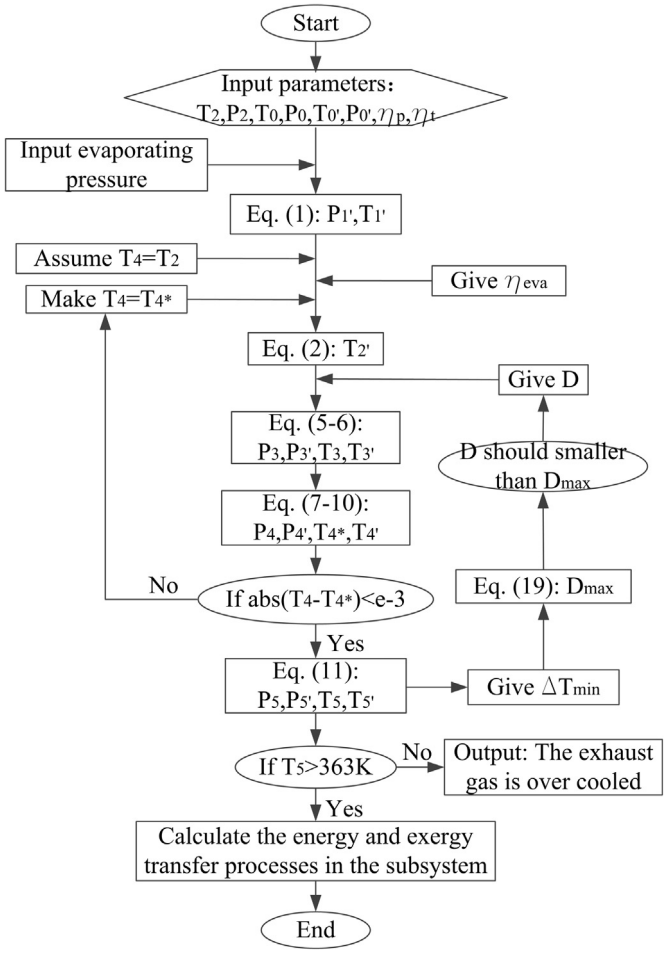

Fig. 5. Flow chart of the simulation procedure.

with the engine 1D simulation software GT-Power developed by Gamma Technologies Inc [30].

A turbocharged diesel engine was selected, and the main parameters are shown in Table 1. In the simulation processes, the heat release rate curve in the cylinder was fitted with the Wiebe model, the cylinder heat transfer process was solved with the Woschni model, and the mechanical friction of the engine was calculated based on the Chen-Flynn model. For more detailed information, please refer to the GT-power user's manual. As shown in Fig. 6 and Fig. 7, the primary simulation data under full load operating conditions in the entire speed range (from 800 r/min to 2200 r/min) including the brake power, BSFC (brake specific fuel consumption), air mass flow rate and compressor pressure ratio, are calibrated with the experimental data, and the maximum error is no larger than 5%, which shows great agreement.

Since the turbocharger plays an important role in the WHR system, the full load operating points on the compressor map before and after steam injection should be compared seriously. It is worth mentioned that the compressor pressure ratios at high speed operating points (from 1800 r/min to 2200 r/min) almost are equal as shown in Fig. 7, which means this turbocharger is equipped with a wastegate to control the boost pressure. Also the wastegate has become a widespread approach to match the operating conditions between the engine and the turbocharger [31]. Since the wastegate bypasses a portion of the exhaust flow before the turbine wheel, we removed the wastegate object in the GT-power model to keep the injected steam form being wasted in the following simulation. The pre-turbine steam injection was modeled by adding an injector object before the turbine with a constant mass flow rate of the injected steam, and advancing the IVC timing was adopted to guarantee the air mass flow at the original operating level. Since the fuel injection parameters were kept constant, the assumption that the heat release curve remained the same was reasonable.

4. Results and discussions

4.1. Influences of injected parameters

Ignoring the pressure drops in pipes, the injected steam pressure, which should be larger than that of the exhaust gas before the turbine, is equal to the evaporating pressure. Here we assumed the evaporating pressure was fixed at 5 bar, the injected mass flow ratio ranged from 0 to 0.15, and the evaporation efficiency ranged from 0.4 to 0.9. Fig. 8 shows influences of the injected mass flow ratio, which represents the mass flow rate of the injected steam, and the evaporation efficiency, which indicates the temperature of the injected steam, on the exhaust gas utilization efficiency. The conclusions can be drawn as follows.

1) The exhaust gas utilization efficiency increases with the increase of the mass flow rate and the temperature of the injected steam, which can be improved from 0.21 to 0.28 under the selected operating conditions, and the corresponding turbine output approximately increases by 33%.

Table 1
Engine specifications.

Type	Four-stroke, six-cylinder, turbocharged, diesel engine
Bore × stroke	114 × 135 mm
Compression ratio	17.7:1
Displacement volume	1.38 l/cylinder
Rated power	183 kW@2200 r/min
Maximum torque	955 Nm@1300 r/min

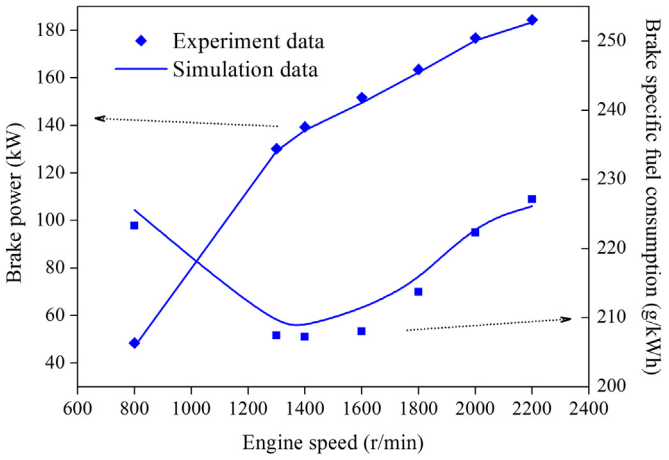

Fig. 6. Calibration of operating points on compressor map.

2) Judging from the contour lines of the exhaust gas utilization efficiency, the effect of the injected mass flow rate is much larger than that of the injected temperature.
3) The dotted line shows the constraint relationship between the injected mass flow rate and the injected temperature when the MTD is set at 10 K, which indicates that a small increase of the injected mass flow rate will cause a sharp decrease of the injected temperature under the same MTD condition.
4) Comparing the gradients between the contour lines and the dotted line, the high injected temperature with the low injected mass flow rate achieve a high exhaust gas utilization efficiency when the MTD of the evaporator is fixed.

In order to improve the exhaust gas utilization efficiency, effects of every injected parameter on the exergy destruction of the exhaust gas WHR subsystem should be investigated singly.

Fig. 9 shows influences of the injected mass flow ratio on the exergy destruction rates of the subsystem when the evaporation efficiency and the evaporating pressure are set at 0.8 and 5 bar. With the increase of the steam mass flow rate and the fixed injected

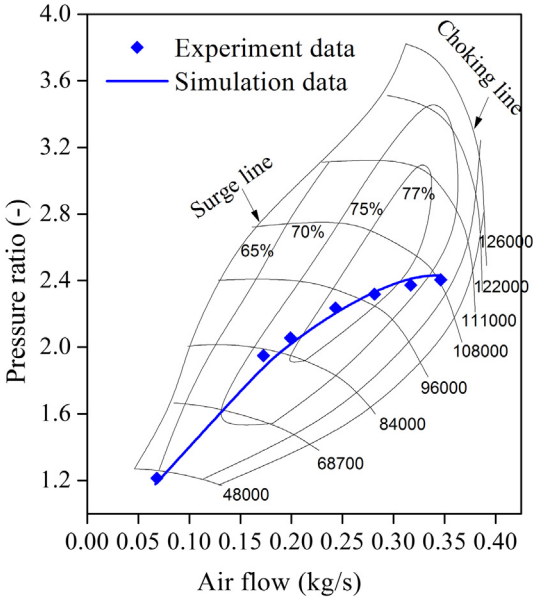

Fig. 7. Calibration of brake power and brake specific fuel consumption.

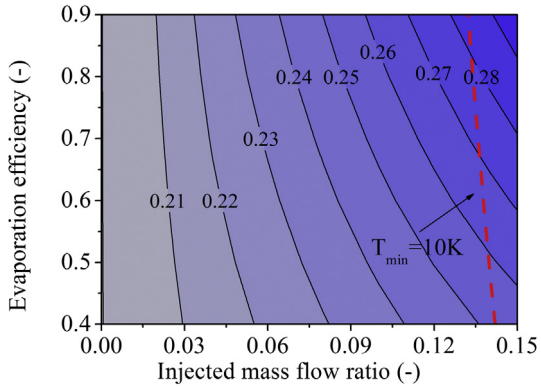

Fig. 8. Contour map of the exhaust gas utilization efficiency.

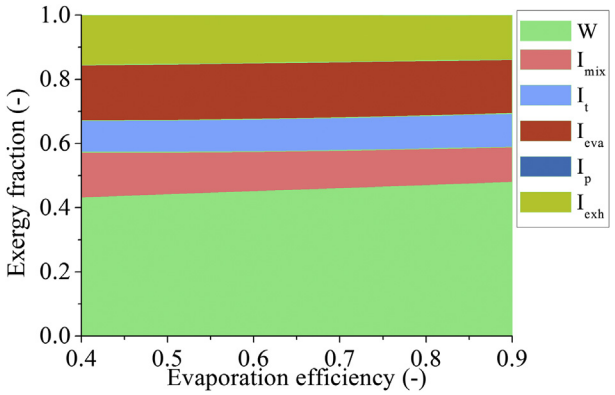

Fig. 10. Effect of the evaporation efficiency on exergy distributions.

temperature and injected pressure, the exergy destruction rates of the mixing process and the evaporating process increase, the exergy destruction rate of the expansion process remains almost the same, and the exergy destruction rate of the discharging process decreases. The two kinds of exergy destruction in the mixing and evaporating processes become the main obstacle for improving the subsystem efficiency and almost are equal in quantity. Also considering from viewpoint of energy balance, although the increase of the injected mass flow rate will decrease the temperature before the turbine, the turbine outlet temperature will also decrease if the turbine expansion ratio changes very little according to Eqs. (6) and (10). Thus the injected mass flow rate plays a dominated role in Eq. (9), which results a linear increase of the turbine output power.

Another important injected parameter is the temperature of the injected steam. Fig. 10 shows effects of the evaporation efficiency on the exergy destruction rates of the subsystem when the injected mass flow ratio and the evaporating pressure are assumed to be 0.1 and 5 bar. With the increase of the injected temperature and the fixed steam mass flow rate and injected pressure, the exergy destruction rates of the mixing process and the discharging process decrease slightly due to the high temperature of the superheated steam, which improve the turbine output power linearly but slowly. Effects of the injected temperature concluded from the exergy analysis agree well with those results shown in Fig. 6.

Fig. 11 shows effects of the evaporating pressure on the exergy destruction rates of the subsystem when the injected mass flow ratio and the evaporation efficiency are set to be 0.1 and 0.8. With the increase of the evaporating pressure and the fixed steam mass flow rate and injected temperature, the exergy destruction rate of the evaporating process decreases slowly due to the decrease of the temperature difference between the hot and cold sides of the evaporator. At the same time, a high injected pressure causes a high pressure energy loss in the steam injection process, which increases the exergy destruction rate of the mixing process. Due to those two factors, the injected pressure shows little influence on the turbine output power. Considering from the viewpoint of energy balance, the pressure has little influence on the enthalpy of the superheated steam since the high temperature superheated steam can be approximately regarded as the ideal gas. Thus the evaporating pressure almost has no effect on the enthalpy of the wet gases before the turbine, which makes the turbine output power change slightly. Also the evaporating pressure should not be too high from the cost-effective view.

4.2. Engine performances

As has been mentioned above, the turbocharger is equipped with a wastegate to control the boost pressure. So three operating cases were conducted and compared with the original case, which can be described as follows: the wastegate was removed in case 1 to show its effects on boost pressures at high speed operating points; the pre-turbine steam injection without the wastegate was adopted in case 2 to investigate changes of the full load operating points with excessively large air mass flow; the pre-turbine steam injection without the wastegate and the adjustment of IVC timing were applied in case 3 to validate the feasibility of this new in-cylinder WHR system. The injected mass flow ratio and the evaporation efficiency in case 2 and case 3 were set to be 0.1 and 0.8, respectively. The IVC strategy in case 3 was achieved by advancing the IVC

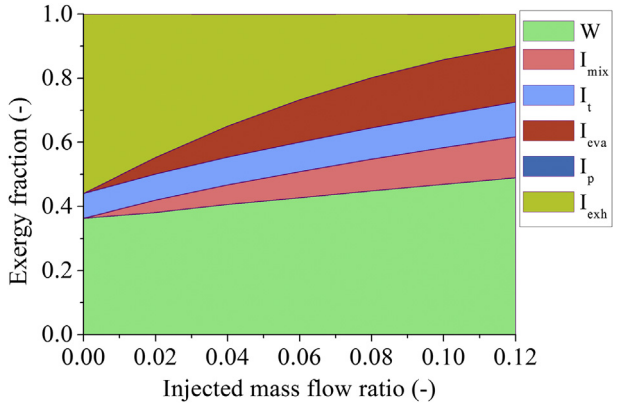

Fig. 9. Effect of the injected mass flow ratio on exergy distributions.

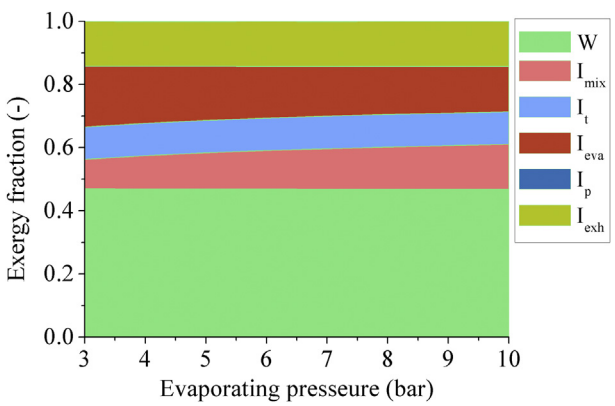

Fig. 11. Effect of the evaporating pressure on exergy distributions.

timing 55°CA (crank angle) to control the air mass flow within the compressor map range, and the intake valve profile is shown in Fig. 12. To control the air mass flow at the original operating level, different IVC timings should be adopted at different engine speeds. In this study, only one IVC timing, which was selected based on the high speed operating conditions, was adopted to simplify the simulation process.

Fig. 13 shows variations of the full load operating points on the compressor map. Without the wastegate in case 1, the operating points at 2000 r/min and 2200 r/min move towards the choking line. With the pre-turbine steam injection in case 2, all the full load operating points move towards the upper right, and the operating points of 2000 r/min and 2200 r/min stand on the choking line since the flow in the compressor becomes sonic. With the adjustment of the IVC timing in case 3, the volumetric efficiencies at high speed operating points decrease dramatically, which draws the high speed operating points back into the compressor map range. Compared case 3 with the original case, the EIVC (early intake valve close) strategy (EIVC = 55°CA) controls the air mass flow at high speeds as the original level and makes the air mass flow at low speeds smaller than the original level. So optimizing IVC timings at different engine speeds is necessary to be conducted but is not included in this research paper.

Fig. 14 compares the turbine shaft power and expansion ratios at full load operating points of the four cases. It can be seen that the turbine shaft power and the expansion ratio almost have the same variation tendency. After removing the wastegate in case 1, more exhaust gas at high speed operating points flows into the turbine, which results higher expansion ratios and larger shaft power. The pre-turbine steam injection in case 2 has the same effect on the expansion ratio and shaft power. With the EIVC strategy in case 3, the charge air mass flow is restricted, and the turbine expansion ratio and shaft power fall down to the case 1 level. Compared case 3 with the original case, the increments of the compressor pressure ratio are larger than those of the turbine expansion ratio, which validates the *P–V* diagram in Fig. 3.

Fig. 15 shows the brake power and BSFC under full load conditions of the four cases. With the pre-turbine steam injection in case 2, the BSFC at high speed operating points (2000 r/min and 2200 r/min) is deteriorated due to the low turbocharger efficiency, and the BSFC at low speed operating points (from 800 r/min to 1600 r/min) decreases apparently owing to the larger air mass flow. With the EIVC strategy in case 3, the BSFC at high speed operating points (from 1800 r/min to 2200 r/min) decreases obviously due to the high pumping efficiency, and the BSFC at low speed operating points (from 800 r/min to 1400 r/min) increases owing to the decreased air mass flow. Since the fuel injection parameters were kept constant during the simulation process, the brake power has the similar variation with the BSFC.

Thus to optimize the BSFC under full load conditions, the pre-turbine steam injection combined with the EIVC strategy should be adopted at high speed operating points, and only the pre-turbine steam injection should be adopted at low speed operating points. With the injected mass flow ratio of 0.1 and the EIVC timing of 55°CA, the BSFC under the rated operating condition can be improved by 3.2%. To further decrease the BSFC, more superheated steam should be injected, but the original compressor map may not have a sufficient pressure ratio range. So the maximum value of the injection mass flow ratio is set to be 0.1 because of the original compressor map range. In order to make full use of this new WHR system, it is necessary to reselect a turbocharger with high efficiency and high pressure ratio.

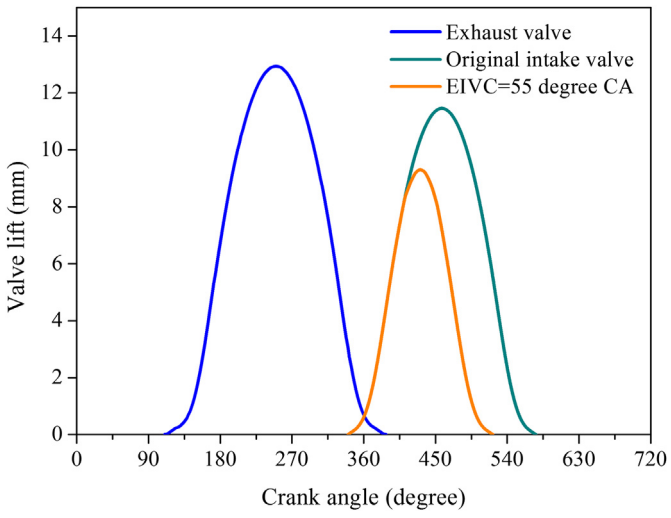

Fig. 12. Valve profile of EIVC strategy.

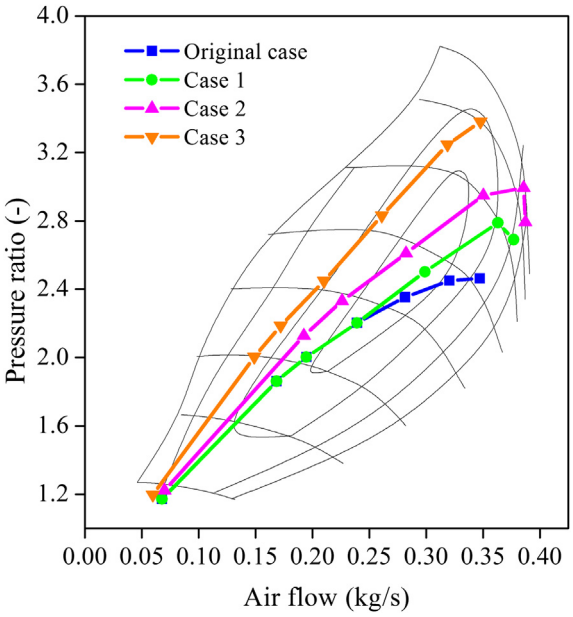

Fig. 13. Comparison of operating points on compressor map.

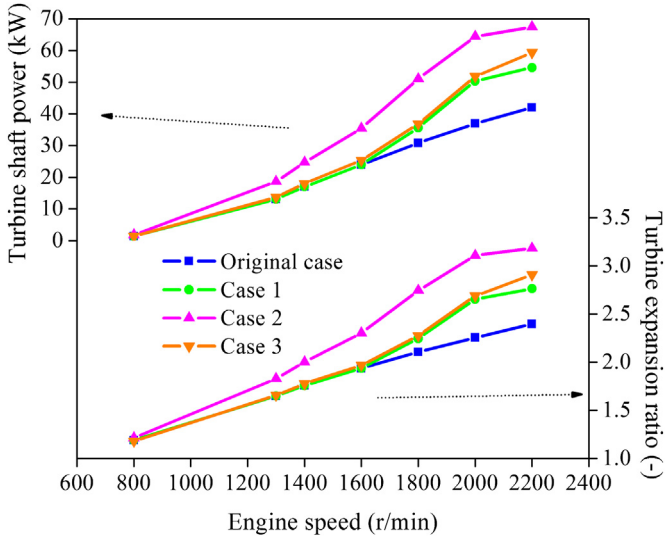

Fig. 14. Comparison of turbine shaft power and expansion ratio.

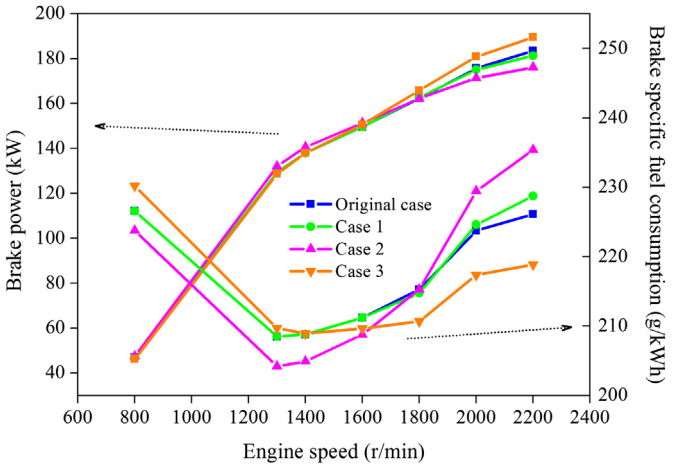

Fig. 15. Comparison of brake power and brake specific fuel consumption.

5. Conclusions

Different from the traditional bottoming Rankine cycle system, an in-cylinder WHR system was proposed in this paper, which can be easily achieved with a relatively simple configuration. According to the thermodynamic analyses and simulation results, the following conclusions are obtained.

1 Among the three injected parameters, the injected mass flow rate has the biggest influence on the recovery efficiency followed by the injected temperature and the injected pressure, and a restricted relationship between the injected mass flow rate and the injected temperature can be obtained with a fixed MTD of the evaporator.
2 The exergy destruction rates of the mixing process and the evaporating process occupy the main parts of the overall exergy destruction rate, which seriously deteriorate the exhaust gas utilization efficiency and cannot be eliminated.
3 If only the pre-turbine steam injection is adopted under full load conditions, the BSFC will be deteriorated at high speed operating points and be improved at low speed operating points. Combined with the adjustment of IVC timing (EIVC = 55°CA), the fuel economy can be improved by 3.2% under the rated operating condition when the injected mass flow ratio is set to be 0.1.
4 The fuel economy can be further improved with more injected steam, optimized IVC timings and a new turbocharger with high efficiency and large pressure ratio.

This paper is focused on the thermodynamic analyses to validate the feasibility of the in-cylinder WHR system under the full load operating conditions of a turbocharged diesel engine. Simulation and experimental researches will be conducted to optimize the control strategies of the injected parameters and the IVC timings and to study influences of this in-cylinder WHR system on the fuel economy, NOx emissions and turbocharger performances under the whole operating conditions in the near future.

Acknowledgments

This work was sponsored by the National Pre-Research Project (Project No. 62201020203) during the 12th Five-Year Plan Period.

References

[1] Hussain QE, Brigham DR, Maranville CW. Thermoelectric exhaust heat recovery for hybrid vehicles. SAE technical paper 2009-01-1327.
[2] Yu C, Chau KT. Thermoelectric automotive waste heat energy recovery using maximum power point tracking. Energy Convers Manag 2009;50:1506–12.
[3] Hountalas DT, Katsanos CO, Lamaris VT. Recovering energy from the diesel engine exhaust using mechanical and electrical turbocompounding. SAE technical paper 2007-01-1563.
[4] Arias DA, Shedd TA, Jester RK. Theoretical analysis of waste heat recovery from an internal combustion engine in a hybrid vehicle. SAE technical paper 2006-01-1605.
[5] Boretti A. Recovery of exhaust and coolant heat with R245fa organic Rankine cycles in a hybrid passenger car with a naturally aspirated gasoline engine. Appl Therm Eng 2012;36:73–7.
[6] Ringler J, Seifert M, Guyotot V, Hübner W. Rankine cycle for waste heat recovery of IC engines. SAE technical paper 2009-01-0174.
[7] Briggs TE, Wagner R, Edwards KD, Curran S, Nafziger E. A waste heat recovery system for light duty diesel engines. SAE technical paper 2010-01-2205.
[8] Yu G, Shu G, Tian H, Wei H, Liu L. Simulation and thermodynamic analysis of a bottoming Organic Rankine Cycle (ORC) of diesel engine (DE). Energy 2013;51:281–90.
[9] Gao W, Zhai J, Li G, Bian Q, Feng L. Performance evaluation and experiment system for waste heat recovery of diesel engine. Energy 2013;55:226–35.
[10] Saidur R, Rezaei M, Muzammil WK, Hassan MH, Paria S, Hasanuzzaman M. Technologies to recover exhaust heat from internal combustion engines. Renew Sustain Energy Rev 2012;16:5649–59.
[11] Wang T, Zhang Y, Peng Z, Shu G. A review of researches on thermal exhaust heat recovery with Rankine cycle. Renew Sustain Energy Rev 2011;15:2862–71.
[12] Sprouse C, Depcik C. Review of organic Rankine cycles for internal combustion engine exhaust waste heat recovery. Appl Therm Eng 2013;51:711–22.
[13] Conklin JC, Szybist JP. A highly efficient six-stroke internal combustion engine cycle with water injection for in-cylinder exhaust heat recovery. Energy 2010;35:1658–64.
[14] Fu J, Liu J, Ren C, Wang L, Deng B, Xu Z. An open steam power cycle used for IC engine exhaust gas energy recovery. Energy 2012;44:544–54.
[15] Serrano JR, Dolz V, Novella R, García A. HD Diesel engine equipped with a bottoming Rankine cycle as a waste heat recovery system. Part 2: evaluation of alternative solutions. Appl Therm Eng 2012;36:279–87.
[16] Fu J, Liu J, Yang Y, Ren C, Zhu G. A new approach for exhaust energy recovery of internal combustion engine: steam turbocharging. Appl Therm Eng 2013;52:150–69.
[17] Liu JP, Fu JQ, Ren CQ, Wang LJ, Xu ZX, Deng BL. Comparison and analysis of engine exhaust gas energy recovery potential through various bottom cycles. Appl Therm Eng 2013;50:1219–34.
[18] Shu G, Zhao J, Tian H, Liang X, Wei H. Parametric and exergetic analysis of waste heat recovery system based on thermoelectric generator and organic rankine cycle utilizing R123. Energy 2012;45:806–16.
[19] Yamada N, Mohamad MNA. Efficiency of hydrogen internal combustion engine combined with open steam Rankine cycle recovering water and waste heat. Int J Hydrogen Energy 2010;35:1430–42.
[20] He M, Zhang X, Zeng K, Gao K. A combined thermodynamic cycle used for waste heat recovery of internal combustion engine. Energy 2011;36:6821–9.
[21] Yan J, Wang Y. Engineering thermodynamics. 2 ed. Beijing, China: China Electric Power Press; 2007 [in Chinese].
[22] Miller RH. Supercharging and internal cooling cycle for high output. Trans ASME 1947;69:453–7.
[23] Tinschmann G, Taschek M, Haberland H, Eilts P. Combustion system development for IMO Tier 2. In: CIMAC Congress, Vienna; 2007. Paper NO.148.
[24] Tagai T, Mimura T, Goto S. Emission control technology by NIIGATA, the clean marine diesel engine for low speed, medium speed and high speed. In: CIMAC Congress, Bergen; 2010. Paper NO.136.
[25] Kim K-D, Yoon W-H, Ghal S-H, Kim H-I, Bae C-S. Optimization of combustion system to comply with IMO Tier 2 regulation on HYUNDAI HiMSEN engines. In: CIMAC Congress. Bergen; 2010. Paper NO.201.
[26] Niemi S, Nousiainen P, Lassila P, Tikkanen V, Ekman K. Effects of Miller timing on the performance and exhaust emissions of a non-road diesel engine. In: CIMAC Congress, Bergen; 2010. Paper NO.52.
[27] Okamoto K, Mori D, Nakazono T, Takemoto T, Kamata M. Development of a 350kW high-efficiency (over 43 %) lean burn gas engine for co-generation systems. In: In CIMAC Congress, Kyoto; 2004. Paper NO.98.
[28] Li Y-R, Wang J-N, Du M-T. Influence of coupled pinch point temperature difference and evaporation temperature on performance of organic Rankine cycle. Energy 2012;42:503–9.
[29] REFPROP version 7.1, NIST standard reference database 23. America: The U.S. Secretary of Commerce; 2003.
[30] Gamma Technologies Inc. GT-POWER V6.2 user's manual, wwwgtisoftcom [retrieved September 20, 2013].
[31] Heywood JB. Internal combustion engine fundamentals. New York: McGraw-Hill; 1988.